

# Parallel Quadtree Construction on Collections of Objects

John Edwards and Nathan Vollmer and Nicholas Harrison

Idaho State University

---

## Abstract

*We present a parallel quadtree algorithm that resolves between geometric objects. The quadtree has the property that no quadtree cell intersects more than one labeled object. Previous parallel algorithms either spawn kernels hierarchically, separate points only, or make no hard guarantees of object separation. Our algorithm runs in **complexity?** in the average case and has excellent results in practice. We demonstrate with results on 2D and 3D datasets.*

Categories and Subject Descriptors (according to ACM CCS): Computer Graphics [I.3.5]: Computational Geometry and Object Modeling—Boundary representations Computer Graphics [I.3.6]: Methodology and Techniques—Graphics data structures and data types

---

## 1. Introduction

Constructing quadtrees on objects is an important task with applications to collision detection, distance fields, robot navigation, object description, and other applications. Quadtrees built on objects most often model the objects themselves, providing a space-efficient representation of arbitrarily complex objects. Our work however, centers on using quadtrees to separate, or resolve, collections of closely spaced objects. Using a quadtree, we can model the space between objects, the first step in constructing distance fields, detecting collisions, and computing the generalized Voronoi diagram. Modeling inter-object spacing is computationally straightforward when inter-object spacing is large compared to the world bounding box. Approaches typically involve a uniform grid of the space, which leads to efficient computation using, very often, graphics processors.

Whereas most algorithms are efficient and robust on certain datasets, all algorithms but one [EDPB15] require inordinate amounts of memory on datasets where objects are very closely spaced relative to the size of the domain. The failures occur because the space is uniformly gridded. In such approaches, voxel size must be small enough to resolve object spacings, and if two objects are very close to each other the number of voxels can become prohibitively large.

We present an algorithm to compute a quadtree on arbitrary datasets, including those with closely spaced and intersecting objects. **Keep going...**

The approach applies a distance transform over an

quadtree representation of the objects. Our quadtree, its associated data structure, and our distance transform are novel and optimized to GVD approximation. For the remainder of the paper, “GVD” will refer to the approximated Generalized Voronoi Diagram.

This paper demonstrates GVD computation on data beyond the computational abilities of previous algorithms, unlocking interesting and important applications. Our approach allows GVD-based proximity queries and other applications using a larger class of meaningful datasets.

Our algorithm has three steps:

1. Construct a quadtree on object vertices using Karras’ algorithm [Kar12]
2. Detect quadtree cells that intersect more than one object, which we call “conflict cells” (contribution)
3. Subdivide conflict cells to resolve objects (contribution)

Each step is done in parallel either on vertices, quadtree cells or object facets (lines).

## 2. Related work

Related work falls into two categories: algorithms that compute the GVD and algorithms that compute distance fields, many of which are adaptive.

**Generalized Voronoi diagrams** A theoretical framework for generalized Voronoi diagrams can be found in Boissonnat et al. [BWY06]. Ordinary Voronoi diagrams are well

studied and efficient algorithms exist that compute them exactly [DBCVK08], but exact algorithms for the generalized Voronoi diagram are limited to a small set of special cases [Lee82, Kar04]. In an early work, Lavender et al. [LBD\*92] define and compute GVDs over a set of solid models using an quadtree. Etzion and Rappoport [ER02] represent the GVD bisector symbolically for lazy evaluation, but are limited to sites that are polyhedra. Boada et al. [BCS02, BC-MAS08] use an adaptive approach to GVD computation, but their algorithm is restricted to GVDs with connected regions and is inefficient for polyhedral objects with many facets. Two other works are adaptive [TT97, VO98] but are computationally expensive and are restricted to convex sites.

In recent years Voronoi diagram algorithms that take advantage of fast graphics hardware have become more common [CTMT10, FG06, HT05, RT07, SGGM06, SGG\*06, HIKL\*99, WLXZ08]. These algorithms are efficient and generalize well to the GVD, but most are limited to a subset of site types. More importantly, all of them use uniform grids and require an extraordinary number of voxels to resolve closely spaced objects (for example, Figs. ?? and ?? would require  $2^{36}$  and  $2^{48}$  voxels, respectively). To our knowledge, ours is the first fully adaptive algorithm that computes the generalized Voronoi diagram for arbitrary datasets.

**Distance fields and quadtrees** The GVD is a subset of the locus of distance field critical points, a property that we take advantage of. In that light, the GVD could be a post-processing step to any method that computes a distance field. Distance transforms compute a distance field, but most are uniformly gridded [JBS06] and are thus no more suitable than GVD algorithms that use the GPU.

Two seminal works adaptively compute the Adaptive Distance Field (ADF) on quadtree vertices. Strain [Str99] fully resolves the quadtree everywhere on the object surface, and Frisken et al. [FPRJ00] resolve the quadtree fully only in areas of small local feature size. Both approaches are designed to retain features of a single object rather than resolving between multiple objects, as is required for GVD computation. Qu et al. [QZS\*04] implement an energy-minimizing distance field algorithm that preserves features at the expense of efficiency. Many recent works on fast quadtree construction using the GPU are limited to point sites [BGPZ12, Kar12, ZGHG11]. Most quadtree approaches that support surfaces [BLD13, CNLE09, LK11, LH07] are designed for efficient rendering, and actual construction of the quadtree is implemented on the CPU.

Two works [BC08, PLKK10] implement the ADF using GPU parallelism to compute the distance value at sample points, but building the quadtree itself is done sequentially. Yin et al. [YLW11] compute the distance field entirely on the GPU using a bottom-up approach by initially subdividing into a complete quadtree, resulting in memory usage that is no better than using a uniform grid. A method by Kim and Liu [KL14] computes the quadtree and a BVH entirely

raw	lexsort	lensort
10110	0001	10
11	00101	10
0001	010110	11
10110	0110100	11
10	10	0001
010110	10	00101
10110	10110	10110
00101	10110	10110
0110100	10110	10110
10	11	010110
11	11	0110100

Figure 1: Sorting the SCC-facet pairs. We first sort lexicographically (*lexsort*), then by length (*lensort*), using a parallel radix sort. In the *lexsort*, we implicitly pad with zeros on the right so that all values are the same length. **How exactly is the *lensort* done?**

on the GPU. However, quadtree construction is performed on barycenters of triangles, and so a leaf quadtree cell can have an arbitrary number of triangle intersections as long as it contains no more than one triangle's barycenter. We have found no GPU quadtree construction method that can resolve between objects.

### 3. Algorithm

#### 3.1. Detecting conflict cells

Let the “quadtree address” refer to the unique ID of a quadtree cell  $C$  found by concatenating the local addresses of its ancestors from Root to  $C$ . The address of the root cell is a special case and is defined as  $R$ . Figure 3d shows the addresses of each leaf cell in the quadtree.

We define a smallest containing cell (SCC) to be the smallest internal quadtree node which entirely contains a given facet. Given a facet defined by two endpoints  $p$  and  $q$ , the quadtree address of the SCC is the longest common prefix of the Morton codes of  $p$  and  $q$ . In figure 3c, the address of the SCC of facet D is 10. The SCC of facet E is  $R$ .

We construct an array of facet-SCC pairs, which is the same size as the number of facets. After allocation, SCC discovery for each facet is done in parallel. We call the array the SCC array.

Next we sort the SCC array, which is demonstrated in figure 1. We first sort using a radix lexicographical sort, then sort by SCC address size. This sort is done in parallel with Karras octree construction.

Then we use the SCC array to find the conflict cells using algorithm 2.

**Algorithm 1: FIND\_CONFLICT\_CELLS****Input:** VertexQuadtree

```

1 for leaf cell  $L$  do in parallel
2    $L.color = -1$ 
3   foreach cell  $A$  in  $direct\_ancestors(L)$  do
4      $id := compute\_cell\_index(A)$ 
5     foreach cell2facet in identical elements of
      cells2facets[id] do
6        $f := cell2facet.facet$ 
7       if  $f$  intersects  $L$  then
8         if  $L.color == -1$  then
9           // First facet found
10          // that intersects  $L$ 
11           $L.color = f.color$ 
12           $L.facet[0] = f$ 
13        end
14        else if  $L.color != f.color$  then
15          // Cell  $L$  is ambiguous
16           $L.color = -2$ 
17           $L.facet[1] = f$ 
18        end
19      end
20    end
21  end

```

**3.2. Resolving conflict cells**

A conflict cell is a quadtree cell that intersects at least two different objects. To resolve a conflict cell  $c$ , we consider pairs of lines of differing labels that intersect  $c$ . Figure 2a shows two lines

$$q(t) = q = q_0 + tv \quad (1)$$

$$r(f) = r = r_0 + fw \quad (2)$$

along with a line

$$p(s) = p = p_0 + su \quad (3)$$

that bisects  $q$  and  $r$ . Our strategy will be to sample points  $P$  on  $p(s)$  (figure 2d) such that a quadtree built on  $V \cup P$  will completely “separate”  $q$  and  $r$ , i.e., no descendent cell of  $c$  will intersect both  $q$  and  $r$ . We do this by ensuring that  $P$  is sampled such that every box that intersects both  $q$  and  $r$  also intersects at least two points in  $P$ . Because Karras’ algorithm guarantees that every leaf cell intersects at most one point, we know that no leaf cell will intersect  $q$  and  $r$  and thus no leaf cell will be a conflict cell. We will find a series of boxes such that each box’s left-most intersection with  $p(s)$  is a sample point meeting the above criterion.

We consider only cases where the slope of  $p$  is in the range  $0 \leq m \leq 1$ . All other cases can be transformed to this case

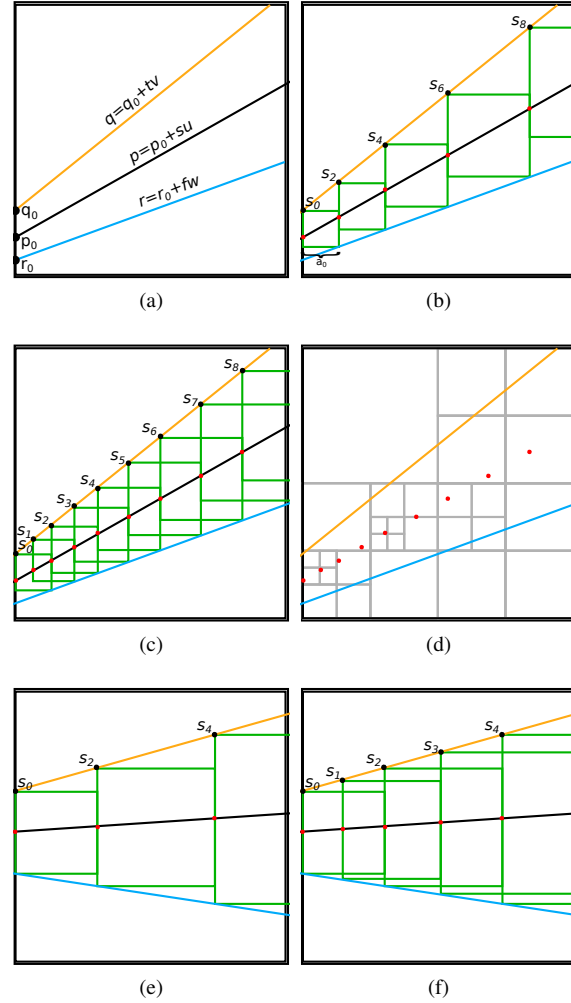


Figure 2: (a) A conflict cell with two lines from different objects. (b) Fitting boxes such that any box intersecting both lines contains at least one sample (red dots). (c) Fitting boxes such that any box intersecting both lines contains at least two samples. This ensures that a quadtree built from the samples using Karras’ algorithm (panel (d)) will have no leaf cells that intersect both lines, ensuring that the new quadtree is locally free of conflict cells.

using rotation and reflection. We begin by fitting the smallest box centered on a point  $p$  that intersects both  $q$  and  $r$ . We break the problem into two cases: the *opposite* case (see Figure 2b) is where  $w^y > 0$ , so each box intersects  $q$  and  $r$  at its top-left and bottom-right corners, respectively. The *adjacent* case (see Figure 2e) is where  $w^y < 0$ , so the line intersections are adjacent at the top-left and bottom-left corners of the box.

### 3.2.1. Finding $a(s)$ – *opposite* case

Given a point  $p(s)$ , we wish to find  $a = a(s)$ , which will give us the starting  $x$  coordinate for the next box. Consider the top-left corner of the box  $q(t(s)) = q(t)$  and the bottom-right corner  $r(f(s)) = r(f)$ .

Because  $p^x(s) = q^x(t)$ ,

$$t = \frac{p^x(s) - q_0^x}{v^x} = \frac{p_x^x - q_0^x + su^x}{v^x} \quad (4)$$

Because our boxes are square,

$$r(f) = r_0 + fw = q_0 + tv + a \begin{bmatrix} 1 \\ -1 \end{bmatrix} \quad (5)$$

From (5),

$$f = \frac{1}{w^y}(q_0^y + tv^y - a - r_0^y) \quad (6)$$

$$a = r_0^x + fw^x - q_0^x - tv^x \quad (7)$$

Substituting equations (4) and (6) into equation (7) and solving for  $a$ ,

$$a(s) = \hat{\alpha}_o s + \hat{\beta}_o \quad (8)$$

where

$$\hat{\alpha}_o = \frac{u^x |w \times v|}{v^x (w^x + w^y)} \quad (9)$$

and

$$\hat{\beta}_o = \frac{|w \times v|(p_0^x - q_0^x) + v^x(|r_0 \times w| + |w \times q_0|)}{v^x (w^x + w^y)} \quad (10)$$

### 3.2.2. Finding $a(s)$ – *adjacent* case

Consider the top-left corner of the box  $q(t(s)) = q(t)$  and the bottom-left corner  $r(f(s)) = r(f)$ .  $r(f)$  is now defined as

$$r(f) = r_0 + fw = q_0 + tv + a \begin{bmatrix} 0 \\ -1 \end{bmatrix} \quad (11)$$

Equations (4) and (6) remain the same while (7) becomes

$$0 = r_0^x + fw^x - q_0^x - tv^x \quad (12)$$

Substituting equations (4) and (6) into equation (12) and solving for  $a$ ,

$$a(s) = \hat{\alpha}_a s + \hat{\beta}_a \quad (13)$$

where

$$\hat{\alpha}_a = \frac{u^x}{v^x w^x} \quad (14)$$

and

$$\hat{\beta}_a = \frac{w^x(p_0^x - q_0^x) + |w \times q_0| + |r_0 \times w|}{w^x} \quad (15)$$

### 3.2.3. Sampling

In both the *opposite* and the *adjacent* cases,  $a(s)$  is of the form  $a(s) = \hat{\alpha}s + \hat{\beta}$ . We now use  $a(s)$  to construct a sequence of  $s$  values  $S = \{s_0, s_1, s_2, \dots, s_n\}$  that meet our sampling criterion. We first construct the even samples (see Figures 2b and 2e). Given a starting point  $p(s_0)$ ,

$$p^x(s_{i+2}) = p^x(s_i) + a(s_i) \quad (16)$$

Substituting in equations (3) and (8)/(13),

$$p_0^x + s_{i+2}u^x = p_0^x + s_i + \hat{\alpha}s_i + \hat{\beta} \quad (17)$$

Solving for  $s_{i+2}$  gives the recurrence relation

$$s_{i+2} = \alpha s_i + \beta \quad (18)$$

where

$$\alpha = 1 + \frac{\hat{\alpha}}{u^x} \quad (19)$$

and

$$\beta = \frac{\hat{\beta}}{u^x} \quad (20)$$

Constructing the odd samples is identical, except that we start at

$$s_1 = \left(1 + \frac{\hat{\alpha}}{2u^x}\right)s_0 + \frac{\hat{\beta}}{2} \quad (21)$$

which is the point in the center of the first box in the  $x$ -dimension.

We solve the recurrence relation (18) using the characteristic polynomial to yield

$$s_i = k_1 + k_2 \alpha^i \quad (22)$$

where

$$k_1^{even} = \frac{\beta}{1 - \alpha} \quad (23)$$

$$k_1^{odd} = \frac{\beta}{1 - \alpha} \quad (24)$$

$$k_2^{even} = \frac{\alpha s_0 + \beta - s_0}{\alpha - 1} \quad (25)$$

$$k_2^{odd} = \frac{\alpha s_1 + \beta - s_1}{\alpha - 1} \quad (26)$$

The last step to formulating  $P$  for parallel computation is to determine how many samples we will need. Let  $p(s_{exit})$  be the point at which the line  $p$  exits the cell.

$$k_1 + k_2 \alpha^i < s_{exit} \quad (27)$$

results in

$$i < \log_{\alpha} \frac{s_{exit} - k_1}{k_2} \quad (28)$$

### 3.3. Build quadtree on vertices

We first construct a quadtree on the vertices of the objects, which we call the “vertex quadtree”. We use Karras’ algorithm [Kar12] which sorts the Morton codes of the vertices in parallel, then constructs the binary radix tree in parallel. With the binary radix tree, the quadtree can be constructed with a single parallel call. The strength of this algorithm lies in the fact that overall performance scales linearly with the number of cores, regardless of the distribution of points. That is, even if a large number of vertices are clustered in a small area, requiring deep quadtree subdivision, only a constant number of parallel calls need be made. Given enough parallel units, the Karras algorithm runs in  $O(\log N)$  time, where  $N$  is the number of vertices.

### 3.4. Identify conflict cells

Our end goal is to construct a quadtree such that no quadtree cell intersects more than one object. Note that a cell is allowed to intersect more than one facet, but all facets must belong to the same object, or, in other words, all facets must share the same label. It is possible, but unlikely, that the vertex quadtree has this property. If so, then we are done. Otherwise, we must identify subdivide conflict cells.

One naive algorithm to identify conflict cells is to process each leaf cell  $c$  in parallel and store which facets intersect  $c$ . This is  $O(N)$ . Another approach is to process each facet in parallel and add it to every cell that it intersects. This is  $O(k \log N)$  where  $k$  is maximum number of cells that any facet intersects. As we will show, our algorithm is  $O(j + \log N)$  where  $j$  is the maximum number of facets that intersect any cell. In practice,  $\log N > j$ , making our algorithm  $O(\log N)$ .

We identify conflict cells as shown in algorithm 2. In lines 1-9, for each internal quadtree cell  $c$ , we store all facets for which  $c$  is the smallest containing cell. Since we are implementing this in a GPGPU environment, we don’t have dynamic memory, so each facet must be processed twice. The first loop discovers how many facets are to be stored in each cell after which we allocate space for the facets. We use parallel prefix sums to determine the amount of space we need to allocate as well as the offsets for each internal cell. The second loop actually stores the facets.

The *container(f)* procedure finds the smallest quadtree cell that fully contains the facet  $f$ . A straightforward implementation of *container(f)* is to perform a standard quadtree search on the vertices of  $f$  and take the smallest quadtree cell that contains all of them. (Note that the cell is always an internal node, since a post-condition of the Karras algorithm is that no leaf cell contains more than one vertex.) In our implementation however, we take advantage of our existing data structures. The quadtree cell that contains a vertex  $v$  is uniquely determined by the D-tuple bits of its morton code. For example, if a 2D vertex has morton code 010010, then

the quadtree is traversed from the root to child 01 to child 00 to child 10. To determine *container(f)*, we find the longest common prefix (*lcp*) of the vertices. Truncating the length of *lcp* to a multiple of  $D$ , we find the smallest quadtree cell that contains all vertices of  $f$ . The complexity of *container(f)* is  $O(\log N)$  for both implementations. Thus, lines 1-9 run in  $O(\log N)$  time.

Lines 10-28 of the algorithm identify and store all facets that intersect with a given leaf cell  $c$ . Again, it is done in two steps for memory allocation purposes. Each leaf cell  $c$  looks at its  $O(\log N)$  ancestors and tests all facets stored in those ancestors for intersection with  $c$ . Any intersecting facets get stored in  $c$ . These lines run in  $O(F)$  time, where  $F$  is the number of facets in all objects. Even though the loop is doubly-nested, each facet is stored in a unique internal node, so no more than  $F$  facets will be visited in the loops. In practice, far fewer than  $F$  facets will be checked for each leaf cell, because most datasets have facets that are completely contained in internal cells that are reasonably low in the tree.

The entire conflict cell detection algorithm runs in  $O(\log N + L) = O(L)$  because  $L > \log N$ . However, average case is  $O(\log N)$ , considering that most lines are contained entirely in a cell at reasonably low depth.

In Step 4, Stack is preallocated to size  $M \cdot 2^D$  where  $M$  is the maximum quadtree depth and  $D$  is the dimension. A conflict cell is a cell that intersects at least two different objects, or two lines of different labels.

The second procedure we use is *direct\_ancestors(c)*, which finds all ancestors of quadtree cell  $c$ .

In Fig. 3, R (Root) is the smallest containing cell for lines A, B, and C, cell 20 contains line D, and cell 2 contains lines E and F. After Step 3 of the algorithm, line A is stored in leaf cells 202, 203, 21, and 3. Conflict cells, which are the only cells that are subdivided, are 203 and 21.

## 4. Compute GVD surface

## 5. Results and applications

Our implementation<sup>†</sup> of the algorithm supports **polygons** and triangulated objects, and our wavefront initialization step is implemented on the GPU using OpenCL. All tests were run on a MacBook Pro laptop with a dual-core 2.9 GHz processor, 8 GB memory, and Intel HD 4000 graphics card. Figure ?? shows our implementation of the GVD computation pipeline, and Figure ?? shows the computed GVD on

<sup>†</sup> Source code is available at <http://cedmav.org/research/project/33-gvds.html>.

**Algorithm 2: FIND\_CONFLICT\_CELLS****Input:** VertexQuadtree

// Store contained facets

```

1 for facet  $f$  in Objects do in parallel
2    $a := \text{container}(f)$ 
3    $a.\text{numFacets} := a.\text{numFacets} + 1$ 
4 end
5 Allocate space for facets in internal cells
6 for facet  $f$  in Objects do in parallel
7    $a := \text{container}(f)$ 
8    $a.\text{facets} := a.\text{facets} \cup f$ 
9 end
10 // Store intersecting facets
11 for leaf cell  $c$  in VertexQuadtree do in parallel
12   foreach cell  $a$  in  $\text{direct\_ancestors}(c)$  do
13     foreach facet  $f$  in  $a.\text{facets}$  do
14       if  $f$  intersects  $c$  then
15          $c.\text{numFacets} := c.\text{numFacets} + 1$ 
16       end
17     end
18   end
19 Allocate space for facets in leaf cells
20 for leaf cell  $c$  in VertexQuadtree do in parallel
21   foreach cell  $a$  in  $\text{direct\_ancestors}(c)$  do
22     foreach facet  $f$  in  $a.\text{facets}$  do
23       if  $f$  intersects  $c$  then
24          $c.\text{facets} := c.\text{facets} \cup f$ 
25       end
26     end
27   end
28 end

```

**Algorithm 3: REFINE\_QUADTREE****Input:** Quadtree, conflict\_cells

// 4. Quadtree refinement

```

1 for leaf cell  $c$  in Quadtree do in parallel
2    $c' := c$ 
3   while  $c' \in \text{conflict\_cells}$  do
4      $(c'_0, c'_1, \dots, c'_{2^d-1}) := \text{subdivide } c'$ 
5     push  $(c'_0, c'_1, \dots, c'_{2^d-1})$  onto Stack
6      $c' := \text{Stack.pop}$ 
7   end
8 end

```

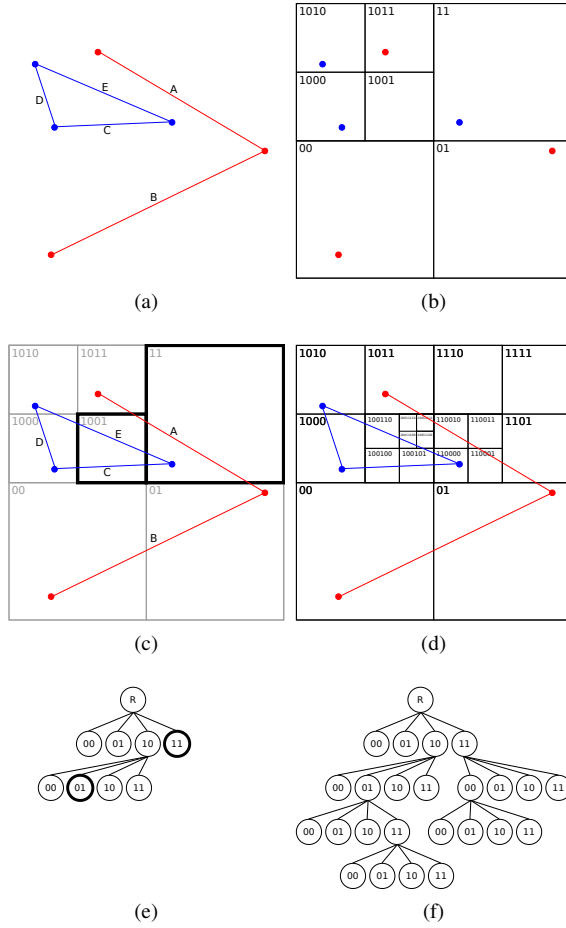


Figure 3: (a) A red object and a blue object. (b) The vertex quadtree, or quadtree built on the object vertices using Karras' algorithm. (c), (e) The vertex quadtree with conflict cells highlighted. Note the label of an quadtree cell in (c) is the concatenation of labels from root R to the leaf cell in (e). This value also corresponds to the highest order bits of the morton code of any point in the cell. (d), (f) The quadtree after resolution of conflict cells.

a more challenging dataset. We compare our method with other work and then show examples in three application settings: path planning, proximity queries, and exploded diagrams.

**5.1. Comparison to other methods****6. Conclusions****References**

[BC08] BASTOS T., CELES W.: Gpu-accelerated adaptively sampled distance fields. In *Shape Modeling and Applications*, 2008.



dataset	objects	object $\Delta s$ ( $\times 10^3$ )	quadtree depth	quadtree cells ( $\times 10^3$ )	quadtree memory (Mb)	GVD (sec)	GVD $\Delta s$ ( $\times 10^3$ )
Fig. ??	3	7	8	54	3	0.9	83
Fig. ??	4	15	12	146	9	3.9	232
Fig. ??	470	5	24	158	8	2.0	151
Fig. ??	448	4015	8	2716	151	195	8100
Fig. ??	35	1500	8	496	70	19	2700

Table 1: Table of quadtree/GVD computation statistics and timings on datasets that are unmanageable using other methods. Columns are: *objects* - the number of objects in the dataset; *object  $\Delta s$*  - the number of line segments (2D) or triangles (3D) of all objects in the dataset; *quadtree depth* - required quadtree depth in order to resolve objects; *quadtree cells* - total number of leaf quadtree cells; *quadtree memory* - amount of memory used by the quadtree; *GVD (sec)* - seconds to perform all steps of GVD computation; *GVD  $\Delta s$*  - number of line segments (2D) or triangles (3D) in the GVD.

- SMI 2008. *IEEE International Conference on* (2008), IEEE, pp. 171–178. 2
- [BCMAS08] BOADA I., COLL N., MADERN N., ANTONI SEL-  
LARES J.: Approximations of 2d and 3d generalized voronoi  
diagrams. *International Journal of Computer Mathematics* 85, 7  
(2008), 1003–1022. 2
- [BCS02] BOADA I., COLL N., SELLARES J.: The voronoi-  
quadtree: construction and visualization. *Eurographics 2002  
Short Presentation* (2002), 349–355. 2
- [BGPZ12] BÉDORF J., GABUROV E., PORTEGIES ZWART S.: A  
sparse octree gravitational-body code that runs entirely  
on the gpu processor. *Journal of Computational Physics* 231, 7  
(2012), 2825–2839. 2
- [BLD13] BAERT J., LAGAE A., DUTRÉ P.: Out-of-core con-  
struction of sparse voxel octrees. In *Proceedings of the 5th High-  
Performance Graphics Conference* (2013), ACM, pp. 27–32. 2
- [BWY06] BOISSONNAT J.-D., WORMSER C., YVINEC M.:  
Curved voronoi diagrams. In *Effective Computational Geome-  
try for Curves and Surfaces*. Springer, 2006, pp. 67–116. 1
- [CNLE09] CRASSIN C., NEYRET F., LEFEBVRE S., EISEMANN  
E.: Gigavoxels: Ray-guided streaming for efficient and detailed  
voxel rendering. In *Proceedings of the 2009 symposium on Inter-  
active 3D graphics and games* (2009), ACM, pp. 15–22. 2
- [CTMT10] CAO T.-T., TANG K., MOHAMED A., TAN T.-S.:  
Parallel banding algorithm to compute exact distance transform  
with the gpu. In *Proceedings of the 2010 ACM SIGGRAPH sym-  
posium on Interactive 3D Graphics and Games* (2010), ACM,  
pp. 83–90. 2
- [DBCVK08] DE BERG M., CHEONG O., VAN KREVELD M.:  
*Computational geometry: algorithms and applications*. Springer,  
2008. 2
- [EDPB15] EDWARDS J., DANIEL E., PASCUCI V., BAJAJ  
C.: Approximating the generalized voronoi diagram of closely  
spaced objects. *Computer Graphics Forum* 34, 2 (2015), 299–  
309. 1
- [ER02] ETZION M., RAPPOPORT A.: Computing voronoi skele-  
tons of a 3-d polyhedron by space subdivision. *Computational  
Geometry* 21, 3 (2002), 87–120. 2
- [FG06] FISCHER I., GOTSCHMAN C.: Fast approximation of high-  
order voronoi diagrams and distance transforms on the gpu. *Jour-  
nal of Graphics, GPU, and Game Tools* 11, 4 (2006), 39–60. 2
- [FPRJ00] FRISKEN S. F., PERRY R. N., ROCKWOOD A. P.,  
JONES T. R.: Adaptively sampled distance fields: a general rep-  
resentation of shape for computer graphics. In *Proceedings of  
the 27th annual conference on Computer graphics and interac-  
tive techniques* (2000), ACM Press/Addison-Wesley Publishing  
Co., pp. 249–254. 2
- [HIKL\*99] HOFF III K. E., KEYSER J., LIN M., MANOCHA D.,  
CULVER T.: Fast computation of generalized voronoi diagrams  
using graphics hardware. In *Proceedings of the 26th annual con-  
ference on Computer graphics and interactive techniques* (1999),  
ACM Press/Addison-Wesley Publishing Co., pp. 277–286. 2
- [HT05] HSIEH H.-H., TAI W.-K.: A simple gpu-based approach  
for 3d voronoi diagram construction and visualization. *Simula-  
tion modelling practice and theory* 13, 8 (2005), 681–692. 2
- [JBS06] JONES M. W., BAERENTZEN J. A., SRAMEK M.: 3d  
distance fields: A survey of techniques and applications. *Visu-  
alization and Computer Graphics, IEEE Transactions on* 12, 4  
(2006), 581–599. 2
- [Kar04] KARAVELAS M. I.: A robust and efficient implemen-  
tation for the segment voronoi diagram. In *International sym-  
posium on Voronoi diagrams in science and engineering* (2004),  
Citeseer, pp. 51–62. 2
- [Kar12] KARRAS T.: Maximizing parallelism in the con-  
struction of bvhs, octrees, and k-d trees. In *Proceedings  
of the Fourth ACM SIGGRAPH/Eurographics conference on  
High-Performance Graphics* (2012), Eurographics Association,  
pp. 33–37. 1, 2, 5
- [KL14] KIM Y. J., LIU F.: Exact and adaptive signed dis-  
tance fields computation for rigid and deformable models on gpus.  
*IEEE Transactions on Visualization and Computer Graphics* 20,  
5 (2014), 714–725. 2
- [LBD\*92] LAVENDER D., BOWYER A., DAVENPORT J., WAL-  
LIS A., WOODWARK J.: Voronoi diagrams of set-theoretic  
solid models. *Computer Graphics and Applications, IEEE* 12,  
5 (1992), 69–77. 2
- [Lee82] LEE D.-T.: Medial axis transformation of a planar shape.  
*Pattern Analysis and Machine Intelligence, IEEE Transactions  
on* (1982), 363–369. 2
- [LH07] LEFEBVRE S., HOPPE H.: Compressed random-access  
trees for spatially coherent data. In *Proceedings of the 18th Eu-  
rographics conference on Rendering Techniques* (2007), Euro-  
graphics Association, pp. 339–349. 2
- [LH11] LAINE S., KARRAS T.: Efficient sparse voxel octrees.  
*Visualization and Computer Graphics, IEEE Transactions on* 17,  
8 (2011), 1048–1059. 2

- [PLKK10] PARK T., LEE S.-H., KIM J.-H., KIM C.-H.: Cuda-based signed distance field calculation for adaptive grids. In *Computer and Information Technology (CIT), 2010 IEEE 10th International Conference on* (2010), IEEE, pp. 1202–1206. [2](#)
- [QZS\*04] QU H., ZHANG N., SHAO R., KAUFMAN A., MUELLER K.: Feature preserving distance fields. In *Volume Visualization and Graphics, 2004 IEEE Symposium on* (2004), IEEE, pp. 39–46. [2](#)
- [RT07] RONG G., TAN T.-S.: Variants of jump flooding algorithm for computing discrete voronoi diagrams. In *Voronoi Diagrams in Science and Engineering, 2007. ISVD'07. 4th International Symposium on* (2007), IEEE, pp. 176–181. [2](#)
- [SGG\*06] SUD A., GOVINDARAJU N., GAYLE R., KABUL I., MANOCHA D.: Fast proximity computation among deformable models using discrete voronoi diagrams. *ACM Transactions on Graphics (TOG)* 25, 3 (2006), 1144–1153. [2](#)
- [SGGM06] SUD A., GOVINDARAJU N., GAYLE R., MANOCHA D.: Interactive 3d distance field computation using linear factorization. In *Proceedings of the 2006 symposium on Interactive 3D graphics and games* (2006), ACM, pp. 117–124. [2](#)
- [Str99] STRAIN J.: Fast tree-based redistancing for level set computations. *Journal of Computational Physics* 152, 2 (1999), 664–686. [2](#)
- [TT97] TEICHMANN M., TELLER S.: Polygonal approximation of voronoi diagrams of a set of triangles in three dimensions. In *Tech Rep 766, Lab of Comp. Sci., MIT* (1997). [2](#)
- [VO98] VLEUGELS J., OVERMARS M.: Approximating voronoi diagrams of convex sites in any dimension. *International Journal of Computational Geometry & Applications* 8, 02 (1998), 201–221. [2](#)
- [WLXZ08] WU X., LIANG X., XU Q., ZHAO Q.: Gpu-based feature-preserving distance field computation. In *Cyberworlds, 2008 International Conference on* (2008), IEEE, pp. 203–208. [2](#)
- [YLW11] YIN K., LIU Y., WU E.: Fast computing adaptively sampled distance field on gpu. In *Pacific Graphics Short Papers* (2011), The Eurographics Association, pp. 25–30. [2](#)
- [ZGHG11] ZHOU K., GONG M., HUANG X., GUO B.: Data-parallel octrees for surface reconstruction. *Visualization and Computer Graphics, IEEE Transactions on* 17, 5 (2011), 669–681. [2](#)